Supporting Information for

Reaction of Ferrate(VI) with ABTS and Self-decay of Ferrate(VI): Kinetics and Mechanisms

Yunho Lee[1,2], Reinhard Kissner[3], Urs von Gunten[1,4,5]*

[1]Eawag, Swiss Federal Institute of Aquatic Science and Technology, Ueberlandstrasse 133, CH-8600 Duebendorf, Switzerland

[2]Department of Environmental Science and Engineering, Gwangju Institute of Science and Technology (GIST), Gwangju 500-712, Republic of Korea

[3]Institute of Inorganic Chemistry, Department of Chemistry and Applied Biosciences, ETH Zurich, CH-8092 Zurich, Switzerland

[4]Institute of Biogeochemistry and Pollutant Dynamics, ETH Zurich, CH-8092 Zurich, Switzerland

[5]School of Architecture, Civil and Environmental Engineering (ENAC), Ecole Polytechnique Fédérale de Lausanne (EPFL), CH-1015, Lausanne, Switzerland

This PDF file includes:

4 texts and 18 figures in 32 pages are available for further information addressing materials, experimental procedures and additional data.

SI-Text-1. Standards and reagents

Potassium ferrate ($K_2Fe^{VI}O_4$) was prepared by the method of Thompson *et al*[1]. In addition, commercially available potassium ferrate (no. 723835) from Sigma-Aldrich was used. These ferrate samples had a purity of 88–98 % as Fe(VI) (w/w) which was determined by dissolving known amounts of solid samples in phosphate buffer solutions (5 mM Na_2HPO_4/ 1 mM borate, pH ≈ 9.2), subsequent filtration through a 0.45 μm nylon syringe filters (BGB Analytik AG, Switzerland), and measuring the ferrate(VI) concentration by both the direct 510 nm method (ε = 1150 $M^{-1}\,cm^{-1}$)[2] and the ABTS method[3]. The remaining 2–12 % of Fe of the prepared potassium

ferrate(VI) were ferric oxides, which was determined by the ferrozine method after reduction of ferric to ferrous ion by hydroxylamine[4]. Stock solutions of ferrate(VI) (0.2–3 mM) were freshly prepared by dissolving solid samples of potassium ferrate(VI) in pure water (pH ≈ 9.2). The fresh stock solution was also quickly filtered through a 0.45 μm nylon syringe filter (BGB Analytik AG, Switzerland) and then standardized spectrophotometrically at 510 nm. Hydrogen peroxide (H_2O_2) stock solutions were prepared from ~30% solutions (Perhydrol, Merck, p.A.). The concentration of H_2O_2 in the stock solution was determined by its UV absorption at 240 nm (ε = 40 M^{-1} cm^{-1})[5]. Fe(II) stock solutions were prepared at 5 mM in 10 mM HCl by using $Fe^{II}Cl_2 \cdot 4H_2O$ and Fe(III) stock solutions were prepared at 5 mM in 10 mM HNO_3 by using $Fe^{III}(NO_3)_3 \cdot 9H_2O$.

SI-Text-2. Reaction kinetics

Kinetic studies of ferrate(VI) reactions were performed in the pH range 1 – 12. For all pH conditions, phosphate (~10 mM for most cases) was used as a buffer as well as a complexing agent for Fe(III). Formation of the soluble Fe(III)-phosphate complexes prevents the precipitation of Fe(III) which might interfere with the optical monitoring of the ferrate(VI) reaction solutions[2]. Together with the phosphate buffer, acetic acid (10 mM) was used as a buffer for the pH range 4.0–5.5 and borate (5 or 10 mM) for the pH range 8.5–9.8. Acetic acid and borate are expected to react very slowly with ferrate(VI) (k << 0.1 M^{-1} s^{-1})[6], therefore does not interfere with the ferrate(VI) reactions of interest under the experimental conditions of this study.

Regarding the influence of the buffers on the fate of perferryl(V) or ferryl(IV) species during ferrate(VI) reactions, phosphate and borate are expected to have a minimal effect considering the low reactivity of these species even to highly reactive OH radicals (k($^{\bullet}OH + H_3BO_3$) = $<5\times10^4$ M^{-1} s^{-1}, and k($^{\bullet}OH + H_2PO_4^-$) = 2×10^4 M^{-1} s^{-1})[7,8]. The influence of acetate is estimated as described below. As the second-order rate constant (k) for the reaction of perferryl(V) with acetate is not known at acidic pH in which acetate is used as a buffer in this study, the k-value known at basic pH (k = 16 M^{-1} s^{-1} at pH 12.4)[9] is used for estimation. As the overall reaction rate for pH > 10 is controlled by the $HFe^{V}O_4^{2-}$ species ($Fe^{V}O_4^{3-}$ shows negligible reactivity)[9], the species-specific k-values for the reaction of $HFe^{V}O_4^{2-}$ with acetate is estimated to be 3×10^3 M^{-1} s^{-1} by taking into account the acid-base equilibrium of perferryl(V) species (i.e., $HFe^{V}O_4^{2-}$ $\Leftrightarrow$ $Fe^{V}O_4^{3-} + H^+$, pK_a = 10.1)[10]. Perferryl(V) undergo another acid-base equilibrium at near-

neutral pH (i.e., $H_2Fe^{V}O_4^{-} \Leftrightarrow HFe^{V}O_4^{2-} + H^{+}$, pK_a = 7.2 – 7.5)[9-11] and $H_2Fe^{V}O_4^{-}$ controls the overall reactivity at pH range 5 – 6. Considering the ~ten-fold larger reactivity (*k*-value) of $H_2Fe^{V}O_4^{-}$ species over $HFe^{V}O_4^{2-}$ species toward gluconic acid (this is the only organic acid species of which the *k*-values are known in the pH range 5–13)[9], the *k*-value for the reaction of $H_2Fe^{V}O_4^{-}$ with acetate is estimated to be 3×10^4 M^{-1} s^{-1}. Using the estimated *k*-value, the consumption rate of Fe(V) by 10 mM acetate at pH 5.5 is 3×10^2 s^{-1}. This rate is ~100-fold lower than the self-decay rate of Fe(V) at this pH ($=4\times10^4$ s^{-1})[11], indicating negligible effect of acetate on the fate of Fe(V) species for the given conditions.

Regarding ferryl(IV) species, a second-order rate constant of <3.1 M^{-1} s^{-1} has been determined for the reaction of ferryl(IV) with acetic acid in 1 M $HClO_4$ solution[12]. Considering the relative higher *k*-value for the reaction of ferryl(IV) with H_2O_2 ($k = 10^4$ M^{-1} s^{-1})[13] and the formation of considerable amount of H_2O_2 during ferrate(VI) reactions (this study), the influence of acetate on the fate of Fe(IV) species is also estimated to be small. All kinetic experiments were performed at room temperature (24±1 °C), except the stopped-flow kinetic experiments which were conducted at 25 °C.

SI-Text-2.1. Reaction of ferrate(VI) with ABTS.

The kinetic studies for the reaction of ferrate(VI) with ABTS were performed with an Applied Photophysics SX–17MV stopped–flow spectrophotometer at 25±0.5°C. Ferrate(VI) solutions were prepared in 5 mM phosphate/1 mM borate buffers at concentrations of 5 μM. ABTS solutions at concentrations of 50 – 400 μM were buffered with 100 mM phosphate or 100 mM phosphate/20 mM acetate at various pH values. Buffered ferrate(VI) and ABTS solutions were then mixed in a 1:1 ratio to initiate the reaction and the formation of $ABTS^{\bullet+}$ was monitored at 415nm**.** The pH was measured after completion of the reaction. Under pseudo-first-order conditions for ferrate(VI), where an excess of ABTS was used ($[Fe(VI)]_0$ = 2.5 μM and $[ABTS]_0$ = 25 – 200 μM), the absorbance increases at 415 nm, which is equivalent to the formation of $ABTS^{\bullet+}$ and ferrate(VI) decrease, followed exponential curves as a function of time, indicating that the reaction is first-order with respect to the ferrate(VI) concentration. Figure SI-1 shows a representative example at pH 3.1.

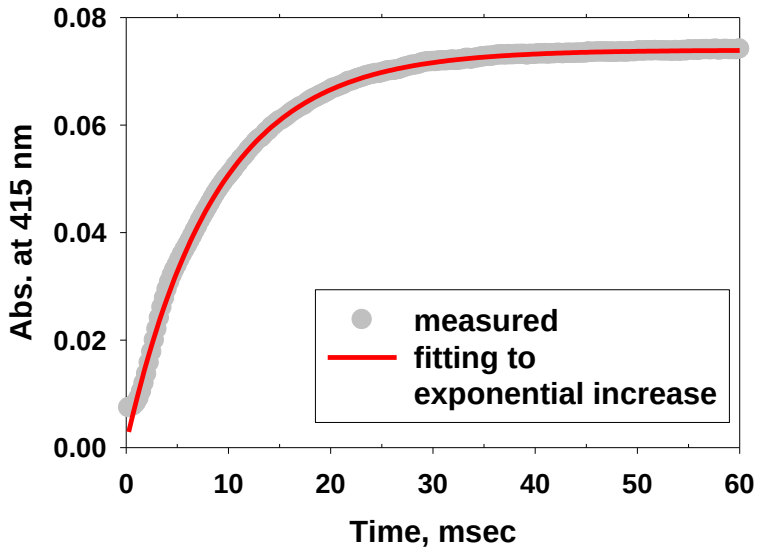

Figure SI-1. Formation of $ABTS^{\bullet+}$ (415nm) from the reaction of 2.5 μM ferrate(VI) with 25 μM ABTS at pH 3.1. The grey circles represent the experimental data and the red line represents the model prediction.

Pseudo-first order rate constants (k_{obs}) were then calculated by an exponential regression (with the SX–17MV operating software) of the average $ABTS^{\bullet+}$ formation curves calculated from at least five replicate curves for each experimental condition. Then, k_{obs} values were determined at various concentrations of ABTS at pH of 3.1, 6.9, and 9.2. Figure SI-2a clearly shows the linearity of k_{obs} with respect to ABTS concentration ($R^2 > 0.99$) and Figure SI-2b confirms the reaction to be first-order with respect to ABTS. Apparent second-order rate constants ($k_{app\text{-}ABTS}$) for the reaction of ferrate(VI) with ABTS were then obtained by dividing the k_{obs} by the ABTS concentration.

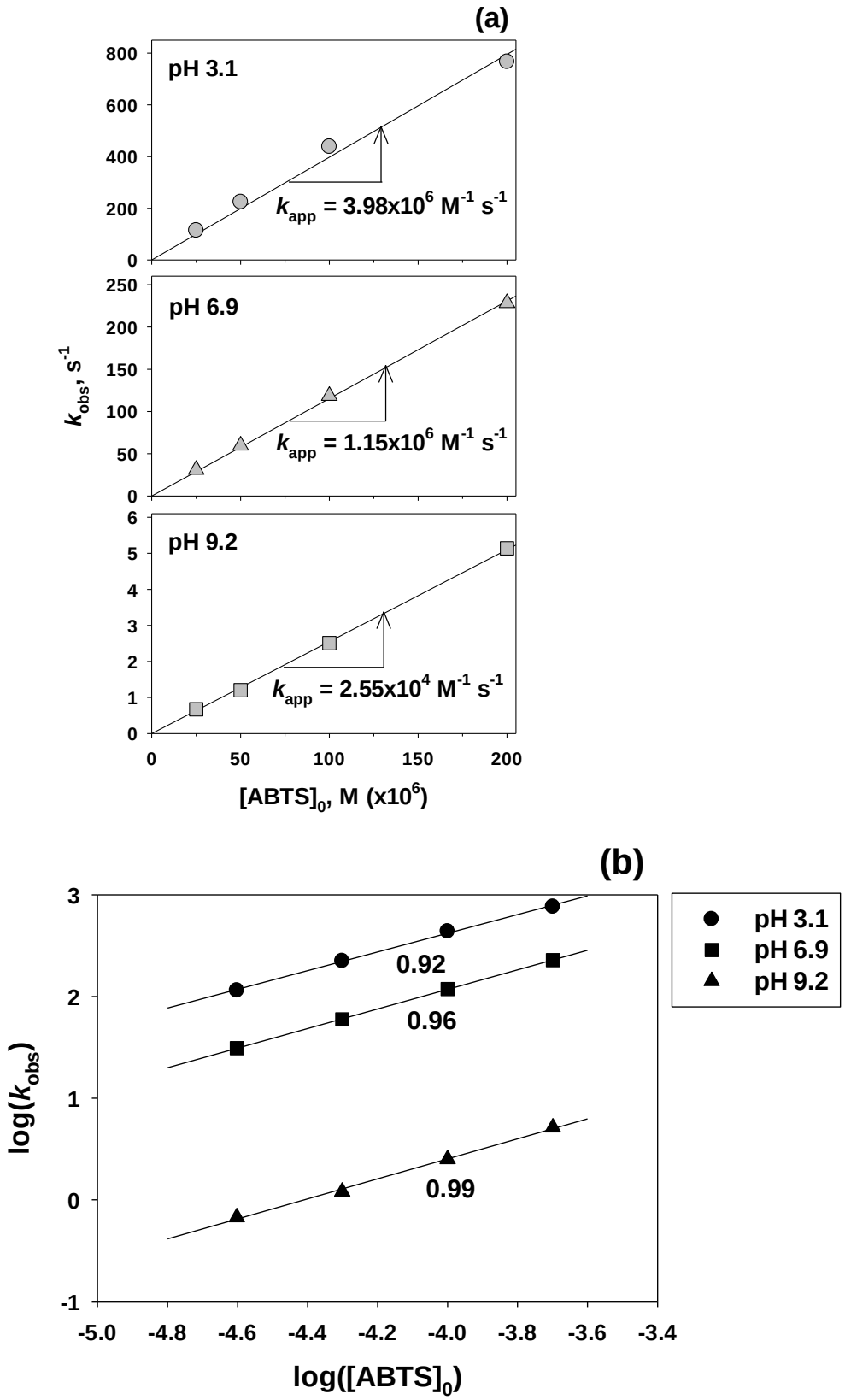

Figure SI-2. (a) Linear and (b) logarithmic plot of the pseudo-first-order rate constant for the formation of $ABTS^{\bullet+}$ (k_{obs}) vs. the initial ABTS concentration at pH 3.1, 6.9, and 9.2. The

symbols represent the experimental data and the line represents the linear fitting of the data. The numbers indicate the slope of the linear fittings.

SI-Text-2.2. Self-decay of ferrate(VI).

Two different methods were used to study the kinetics of the ferrate(VI) self-decomposition. In the first method, the decrease of ferrate(VI) was determined by monitoring the absorbance at 510 nm using a stopped-flow systems. For rapid kinetics (t = 10 ms – 10 s), an Applied Photophysics SX–17MV system was used. For slower reactions (t > 1 s), a Hi-Tech SFA 20 (rapid mixing unit) was used in conjunction with a HP 8452 diode array UV-vis spectrophotometer. For both systems, the temperature was controlled at 25 ± 0.5 °C by a thermostated water bath. Ferrate(VI) solutions were freshly prepared in 5 mM phosphate/1 mM borate buffers at concentrations of 300–500 μM. The reaction solutions (pure H_2O) were buffered with 10 mM phosphate or 10 mM phosphate/10 mM acetate at various pH values. Buffered ferrate(VI) and H_2O solutions were then mixed at 1:1 proportion to initiate the reaction and the decrease of ferrate(VI) was monitored at 510 nm**.** The pH was measured after completion of the reaction. The absorbance decreases at 510 nm were fitted to eq S1 that is derived based on the second-order decay kinetics for ferrate(VI). The fitting was performed by using the software GraphPad Prism (www.graphpad.com).

$$A_{510nm,\,\tau} = \frac{A_{510nm,0}}{1 + 2k_{app\text{-}self}\left[Fe(VI)\right]_0 \tau} \qquad (S1)$$

where $A_{510nm,\,\tau}$ and $A_{510nm,\,0}$ represent an absorbance at 510 nm at a reaction time of τ and zero, respectively ($A_{510nm} = \varepsilon_{510nm} b[Fe(VI)]$ and b = 1 cm), $k_{app\text{-}self}$ represents the apparent second-order rate constant for the self-decomposition of ferrate(VI) at a given pH, and $[Fe(VI)]_0$ represents the initial concentration of ferrate(VI).

Decreases of the 510 nm absorbance were well fitted by eq S1 ($R^2 > 0.98$), indicating that the reaction is second-order with respect to the ferrate(VI) concentration. Figure SI-3 shows representative examples at pH 1.7, 4.0, and 7.2. Second-order rate constants ($k_{app\text{-}self}$) for the self-decay of ferrate(VI) were then calculated from eq S1 and the initial ferrate(VI) concentration. In addition, a molar absorptivity of ferrate(VI) at a given pH could be determined by $\varepsilon_{510nm,pH} = \frac{A_{510nm,0}}{b\left[Fe(VI)\right]_0}$, where $A_{510nm,\,0}$ is the absorbance at 510 nm at a reaction time of zero and calculated from the fitted eq S1. Figure SI-4 shows the measured (circles) and predicted (line) molar absorptivity of ferrate(VI) as a function of pH. The measured $\varepsilon_{510nm,pH}$-values were fitted to an

equation, $\varepsilon_{510nm,pH} = \varepsilon(H_3Fe^{VI}O_4^{+})\alpha_1 + \varepsilon(H_2Fe^{VI}O_4)\alpha_2 + \varepsilon(HFe^{VI}O_4^{-})\alpha_3 + \varepsilon(Fe^{VI}O_4^{2-})\alpha_4$ where $\varepsilon(H_nFe^{VI}O_4^{n-2})$ and α_m represents the molar absorptivity and the fraction of each ferrate(VI) species. During the fitting process, a $\varepsilon(Fe^{VI}O_4^{2-})$ value of 1150 M^{-1} cm^{-1} was used, which is available in literature[2]. The following molar absorptivity values for each ferrate(VI) species were determined (Fig. SI-4): $\varepsilon(H_3Fe^{VI}O_4^{+})$ = 244 (±25), $\varepsilon(H_2Fe^{VI}O_4)$ = 464 (±16), and $\varepsilon(HFe^{VI}O_4^{-})$ = 464 (±16).

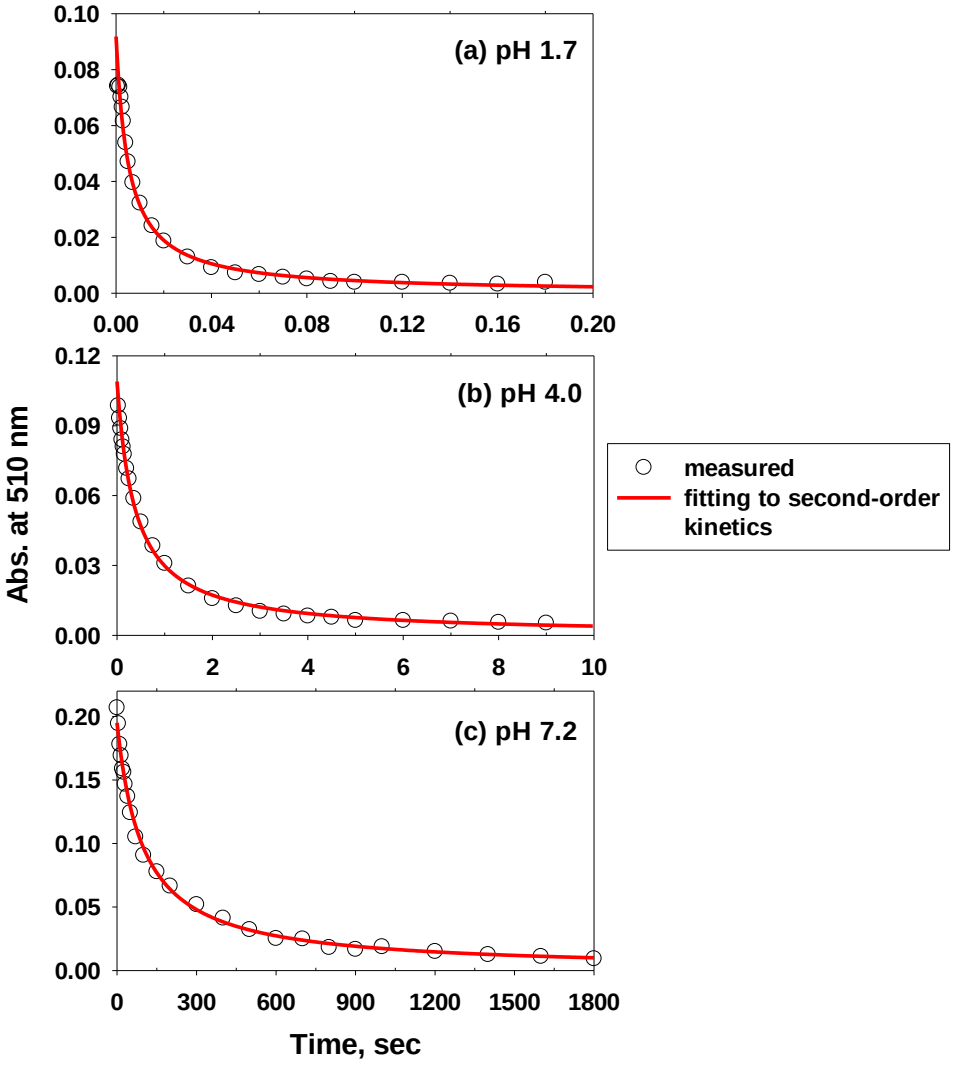

Figure SI-3. Second-order decay curves for ferrate(VI) from the decrease of the absorbance at 510 nm. (a) pH 1.7 and $[Fe(VI)]_0$ = 260 μM, (b) pH 4.0 and $[Fe(VI)]_0$ = 260 μM, and (c) pH 7.2 and $[Fe(VI)]_0$ = 220 μM. Symbols represent experimental data and lines represent model predictions. To improve the visibility of the experimental data, only selected data points are shown.

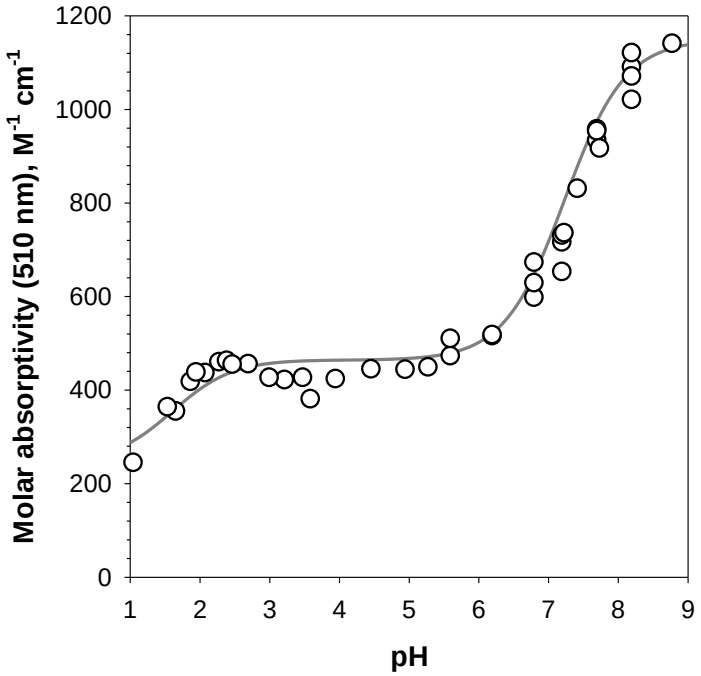

Figure SI-4. Molar absorptivity of ferrate(VI) as a function of pH (1 – 9) at 510nm. The symbols represent the measured data and the lines represent the predicted ones. The measured data were fitted to an equation, $\varepsilon_{510nm,pH} = \varepsilon(H_3Fe^{VI}O_4^{+})\alpha_1 + \varepsilon(H_2Fe^{VI}O_4)\alpha_2 + \varepsilon(HFe^{VI}O_4^{-})\alpha_3 + \varepsilon(Fe^{VI}O_4^{2-})\alpha_4$ where $\varepsilon(H_nFe^{VI}O_4^{n-2})$ and α_m represents the molar absorptivity and the fraction of each ferrate(VI) species.

Secondly, the ABTS method[3] was used to study the kinetics of the self-decomposition of ferrate(VI) (t > 20 s). The reaction was initiated by adding a small volume (<1 mL) of an aliquot of a ferrate(VI) stock solution (~1 mM) to a solution (100 mL) buffered at a desired pH (10 mM phosphate or 10 mM phosphate/acetate mixture) under rapid mixing. At proper time intervals, 1–5 mL of the reaction solution were sampled and quenched with an ABTS solution to measure residual ferrate(VI) concentrations. The apparent second-order rate constants for the ferrate(VI) self-decay ($k_{app\text{-}self}$) were calculated from the slope of the linear curve resulting from a plot of the inverse of the ferrate(VI) concentration vs. the reaction time (τ), which is expressed in eq S2 (eq S2 can be derived from eq S1). Under all experimental conditions, ferrate(VI) decreases were well fitted to eq S2 ($R^2 > 0.98$), confirming that the reaction is second-order with respect to ferrate(VI).

$$\frac{1}{[Fe(VI)]_\tau} = \frac{1}{[Fe(VI)]_0} + 2k_{app\text{-}self}\,\tau \qquad (S2)$$

Figure SI-5 shows the plot of the inverse ferrate(VI) concentration as a function of time at pH 5.5 as a representative data set. The $2k_{app\text{-}self}$ was calculated from the slope of the lines in Figure SI-5 and was independent of the initial Fe(VI) concentration. At pH 5.5, the determined $k_{app\text{-}self}$ was $178 \pm 18\ M^{-1}\ s^{-1}$.

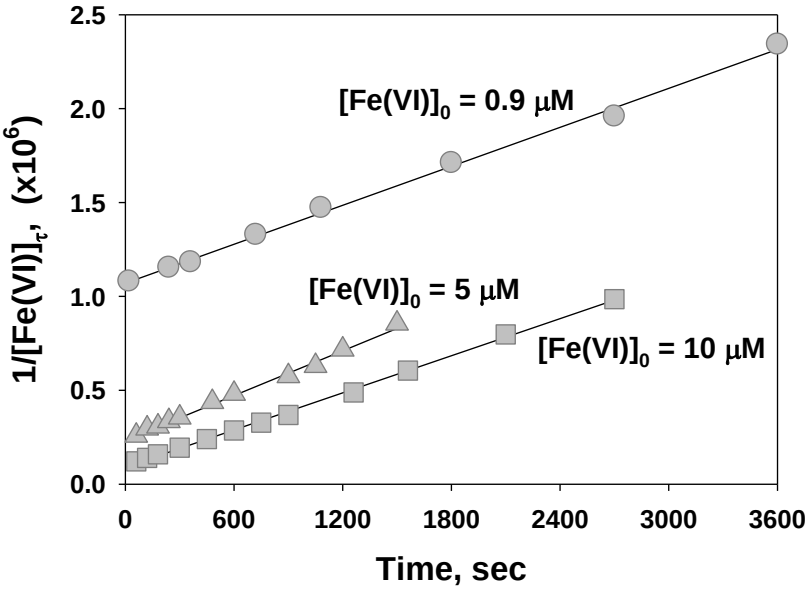

Figure SI-5. Plot of the inverse ferrate(VI) concentration decrease as a function of time during the self-decomposition of ferrate(VI) at pH 5.5. Symbols represent experimental data and lines represent model predictions. $[Fe(VI)]_0$ = 0.9, 5, and 10 μM.

Figure SI-6 compares the Fe(VI) self-decay rate constants ($k_{app\text{-}self}$) determined in this study with literature values. The pH-dependent $k_{app\text{-}self}$ values from this study are comparable within a factor of ~2 in the pH range 2 – 7 to a previous study[14], however, higher than those reported by Sarma et al[15] by a factor of ~4. The difference in the $k_{app\text{-}self}$ values might be attributable to the different phosphate buffer concentrations or ionic strength used in the latter study.

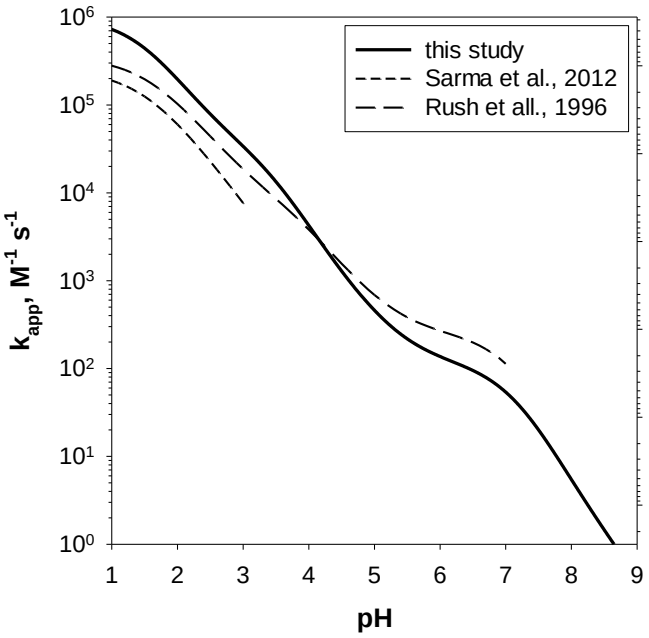

Figure SI-6. Comparison of the second-order rate constants for ferrate(VI) self-decay ($k_{app\text{-}self}$) as a function of pH. The $k_{app\text{-}self}$-values were re-produced using the species-specific *k*-values reported in Rush et al[14] and Sarma et al[15].

SI-Text-2.3. Reaction of ferrate(VI) with H_2O_2.

The kinetics for the reaction of ferrate(VI) with H_2O_2 was investigated by measuring the decrease of ferrate(VI) in presence of excess H_2O_2 ($[Fe(VI)]_0$ = 2 – 10 μM and $[H_2O_2]_0$ = 50 – 680 μM) in the pH range 7 – 12 (10 mM phosphate or 10 mM phosphate/borate mixture). Ferrate(VI) concentrations as a function of time were measured by the ABTS method[3]. Under these conditions, the logarithmic ferrate(VI) concentration decreased linearly with time, indicating that the reaction is pseudo-first-order with respect to the ferrate(VI) concentration. Figure SI-7 shows a representative example at pH 7.0.

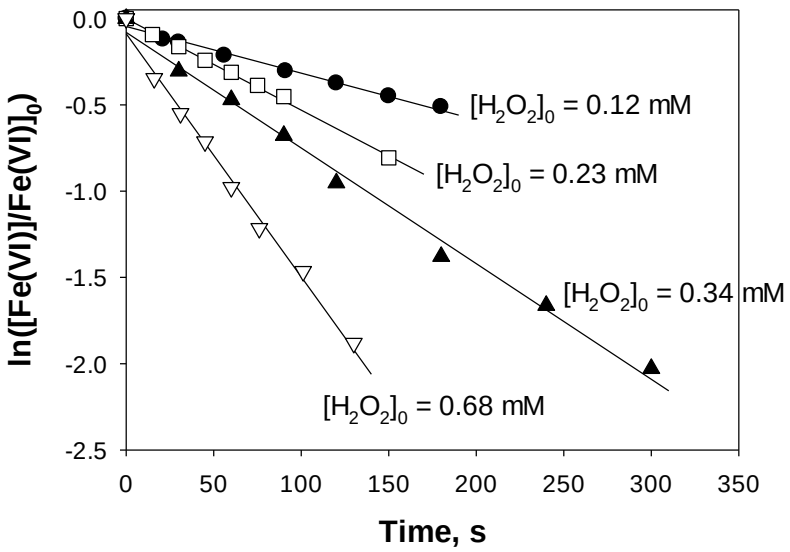

Figure SI-7. Relative logarithmic concentration of ferrate(VI) as a function of the reaction time during the reaction of ferrate(VI) with an excess of H_2O_2 at pH 7.0 ($[Fe(VI)]_0$ = 2 μM and $[H_2O_2]_0$ = 0.12 – 0.68 mM). Symbols represent the experimental data and lines represent the best fits.

Pseudo-first order rate constants (k_{obs}) were calculated from the linear slopes in Figure SI-7. The k_{obs}-values determined at various H_2O_2 concentrations and selected pH conditions (pHs of 7, 9, and 11) are shown in Figure SI-8. In the pH range 7 – 12, k_{obs} increased linearly with increasing H_2O_2 concentration (Figure SI-8a). Figure SI-8b confirms the reaction to be first-order with respect to H_2O_2 because the slope of a plot of log(k_{obs}) vs log($[H_2O_2]$) is close to unity. Apparent second-order rate constants ($k_{app\text{-}H2O2}$) for the reaction of Fe(VI) with H_2O_2 were then obtained by dividing the k_{obs} by the H_2O_2 concentration.

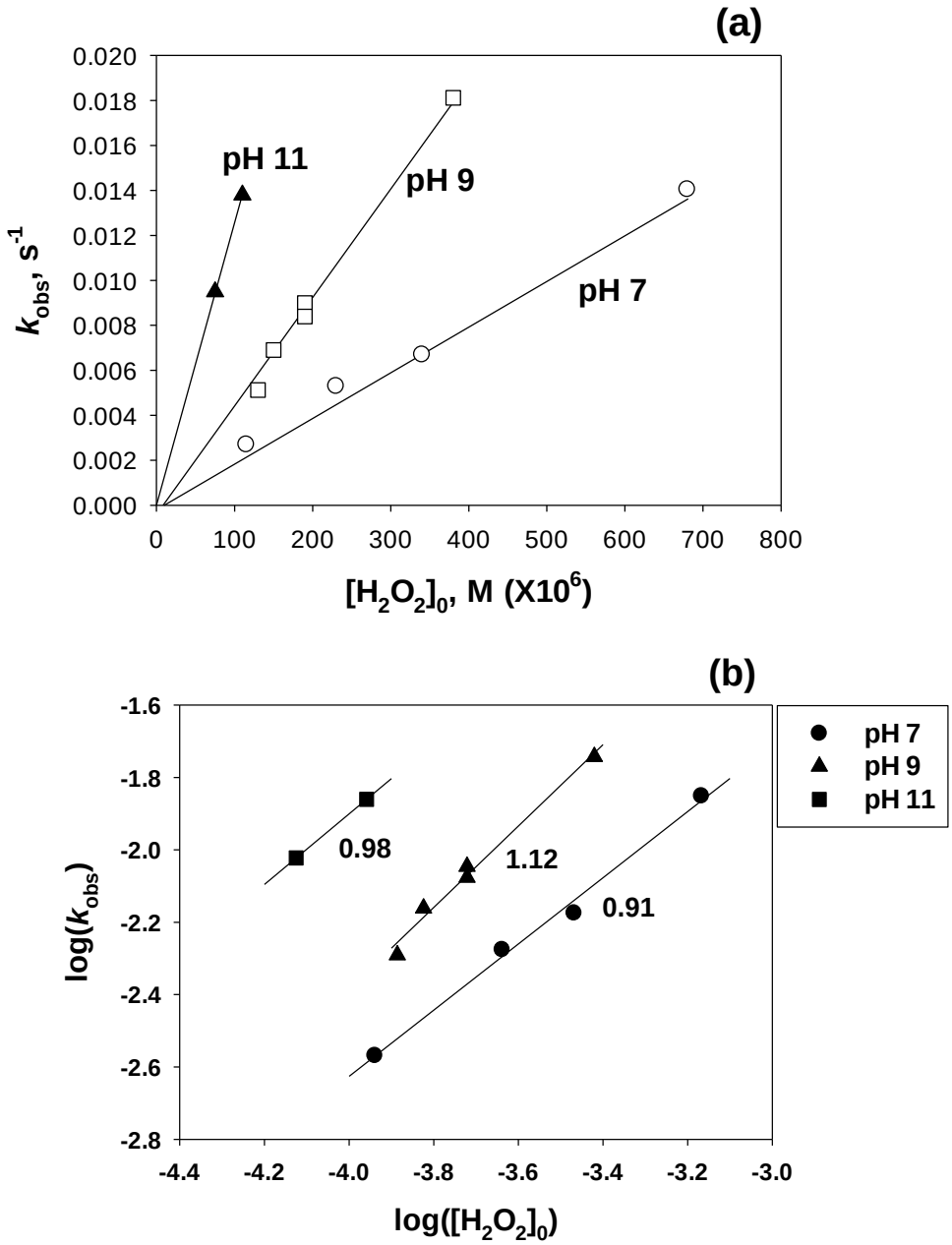

Figure SI-8. (a) Linear and (b) logarithmic plot of the pseudo-first-order rate constant for the decrease of ferrate(VI) (k_{obs}) vs. the initial H_2O_2 concentration at pH 7, 9, and 11. The symbols represent the experimental data and the lines represent linear fits of the data. The numbers indicate the slope of the linear fits.

Figure SI-9 shows the apparent second-order rate constants ($k_{app\text{-}H2O2}$) for the reaction of ferrate(VI) with H_2O_2 as a function of pH (7 – 12). The pH dependence of $k_{app\text{-}H2O2}$ can be explained by considering the speciation of ferrate(VI) (eqs 1 – 3, main text), the speciation of H_2O_2 (eq S3), and the reactions between the Fe(VI) species and the ABTS species.

$$H_2O_2 \rightleftharpoons HO_2^- + H^+ \qquad pK_{H2O2} = 11.6^{16} \qquad \text{(S3)}$$

The species-specific rate constants were determined by a nonlinear least-squares regression of our experimental data ($k_{app\text{-}H2O2}$). The regression results showed that in the tested pH range 7–12, the overall reaction is mainly controlled by the following two reactions S4 and S5.

$$HFe^{VI}O_4^- + HO_2^- \rightarrow \text{products} \qquad k_{H2O2\text{-}3,2} \qquad \text{(S4)}$$

$$Fe^{VI}O_4^{2-} + HO_2^- \rightarrow \text{products} \qquad k_{H2O2\text{-}4,2} \qquad \text{(S5)}$$

The determined rate constants were $k_{H2O2\text{-}3,2} = (1.34\pm0.2)\times10^6$ M^{-1} s^{-1} and $k_{H2O2\text{-}4,2} = (2.3\pm0.2)\times10^2$ M^{-1} s^{-1}. Based on the obtained species specific rate constants, it was found that the reaction between $HFe^{VI}O_4^-$ and HO_2^- ($k_{H2O2\text{-}3,2}\alpha_3\beta_2$) controls the overall reaction within the pH range 7 – 11 and the reaction of $Fe^{VI}O_4^{2-}$ with HO_2^- ($k_{H2O2\text{-}4,2}\alpha_4\beta_2$) becomes important for pH >11.

The pH-dependent $k_{app\text{-}H2O2}$ values were comparable to a previous study in the pH range 9 –12 while lower by up to factor of 8 in the pH range 7 – 9[14]. A significant increase of the $k_{app\text{-}H2O2}$ values was observed in pH < 9 previously[14] while a slight decrease of the $k_{app\text{-}H2O2}$ values was found in our study (Figure 8). This discrepancy might be caused by the different solution compositions in the two studies (i.e., 10 mM phosphate buffer for our study vs 100 mM phosphate buffer with 1 M $NaClO_4$ for Rush et al[14]).

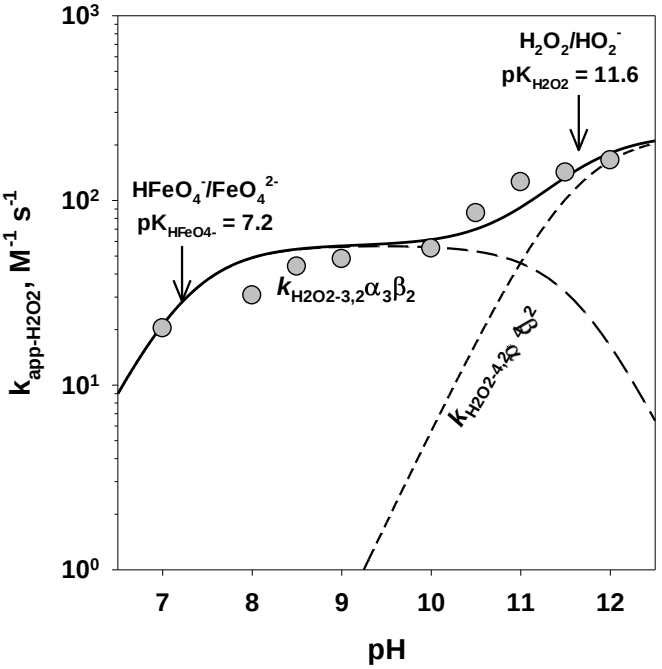

Figure SI-9. Apparent second-order rate constants ($k_{app\text{-}H2O2}$) for the reaction of ferrate(VI) with H_2O_2 in the pH range 7–12 at 24±1°C. The symbols represent the measured data and the lines

represent the model calculations. The dashed lines represent the contribution of the reaction of $HFe^{VI}O_4^-$ with HO_2^- ($k_{H2O2\text{-}3,2}\alpha_3\beta_2$) and $Fe^{VI}O_4^{2-}$ with HO_2^- ($k_{H2O2\text{-}4,2}\alpha_4\beta_2$) to the overall reaction as a function of pH.

SI-Text-2.4. Oxidation of Fe(II) by ferrate(VI).

The kinetics for the oxidation of Fe(II) by ferrate(VI) were investigated with an Applied Photophysics SX–17MV stopped–flow spectrophotometer with temperature controll at 25±0.5°C. Ferrate(VI) solutions were prepared in 1 mM phosphate/10 mM borate buffers at concentrations of 0.2 mM. Fe(II) solutions at concentrations of 2 mM were buffered with 10 mM phosphate/10 mM acetic acid at pH of ~2. Buffered ferrate(VI) and Fe(II) solutions were then mixed in a 1:1 ratio to initiate the reaction and the absorbance at 510 nm was monitored for the decrease of the ferrate(VI) concentration. The pH was measured after the completion of the reaction and was 5. The results showed that the oxidation of Fe(II) by ferrate(VI) was completed within the mixing time of the system (~1 ms) at pH 5.0. Assuming that 99% of the initial ferrate(VI) has reacted with Fe(II) at 1 ms, the second-order rate constant for the reaction of ferrate(VI) with Fe(II) (=k_{15}, see Table 1 in the main text) is >> 5×10^6 M^{-1} s^{-1}. Kinetic simulations showed that the kinetics of O_2 and H_2O_2 formation are independent of the magnitude of k_{15} if it is larger than 5×10^6 M^{-1} s^{-1}. A value of 10^7 M^{-1} s^{-1} was used for k_{15} at pH 7 as a lower limit in the kinetic simulations.

SI-Text-3. Reaction products and stoichiometry

SI-Text-3.1. Reaction of ferrate(VI) with ABTS

20 mL of solutions containing various concentrations of Fe(VI) (2.5 – 31 μM prepared in 5 mM Na_2HPO_4/1 mM borate buffer) were added into each flask of a series containing 5 mL of an ABTS solution (400 μM of ABTS and buffered at the desired pH with 10 mM phosphate or 10 mM phosphate/acetate). After completion of the reaction (it takes less than a few sec based on the determined second-order rate constants, see Fig. 1 in the main text), the consumption of ABTS, the formation of $ABTS^{\bullet+}$ and H_2O_2 were determined within a few minutes.

1) Quantification of ABTS consumption and $ABTS^{\bullet+}$ formation. ABTS has a well-defined absorption maximum at 340 nm ($\varepsilon_{ABTS,\ 340}$ = 3.6×10^4 M^{-1} cm^{-1})[17,18] and does not absorb at 415 nm (Figure SI-10). $ABTS^{\bullet+}$ has an absorption maximum at 415 nm ($\varepsilon_{ABTS\bullet+,415}$ =

$3.6\times10^4\ M^{-1}\,cm^{-1}$)[17,18] and its molar absorption coefficient at 340 nm is $\varepsilon_{ABTS\bullet+,\ 340}$ = $5.4\times10^3\ M^{-1}\,cm^{-1}$ [17,18]. Based on these molar absorption coefficients, the following equations can be derived:

$$\Delta[ABTS^{\bullet+}]_{produced} = \frac{\Delta A_{415}}{\varepsilon_{ABTS\bullet+,415}\ell} \qquad (S6)$$

$$\Delta[ABTS]_{consumed} = \frac{\Delta A_{340}}{\varepsilon_{ABTS,340}\ell} - \frac{\varepsilon_{ABTS\bullet+,340}\Delta[ABTS^{\bullet+}]_{produced}}{\varepsilon_{ABTS,340}\ell} \qquad (S7)$$

where $\Delta[ABTS^{\bullet+}]_{produced}$ and $\Delta[ABTS]_{consumed}$ represent the $ABTS^{\bullet+}$ produced and ABTS consumed, respectively; ΔA_{340} and ΔA_{415} represent the change of the absorbance at 340 and 415 nm, respectively, after completion of the reaction between ferrate(VI) and ABTS; and ℓ represent the optical path-length in the spectrophotometric measurements.

Figure SI-10 shows the UV-Vis spectrum variation after oxidation of ABTS by ferrate(VI). With increasing ferrate(VI) concentration, the absorbance at 340 nm decreased whereas the absorbance at 415 nm increased, which is consistent with the oxidation of ABTS to $ABTS^{\bullet+}$ by ferrate(VI). Consumption of ABTS and formation of $ABTS^{\bullet+}$ were then calculated by eqs S6 & S7 and the measured variations in the absorbance of the treated solution at 340 and 415 nm (ΔA_{340} and ΔA_{415}).

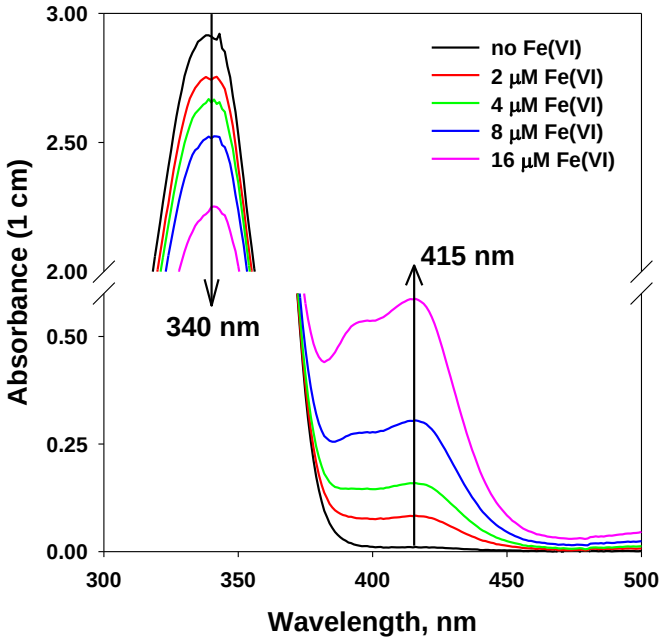

Figure SI-10. Variation in the UV-Vis spectrum after oxidation of ABTS by ferrate(VI). Experimental conditions: $[ABTS]_0$ = 80 μM, $[Fe(VI)]_0$ = 0, 2, 4, 8, and 16 μM (pH = 4.2). For the

determinations of the consumption of ABTS, the absorbance at 340 nm was measured (ΔA_{340}) after dilution of the samples (2 – 4 fold) to minimize errors caused by high absorbance (e.g. A_{340} > 2).

2) Quantification of H_2O_2 formation–the HRP/ABTS method. To measure the formation of H_2O_2, the horseradish peroxidase (HRP)-catalyzed oxidation of ABTS by H_2O_2 was used. The chemistry of the peroxidase-catalyzed oxidation of ABTS by H_2O_2 has been described previously[18] and applied as a method to determine the enzymatic activity of peroxidases[19]. A few studies have also demonstrated that this method can be used to measure H_2O_2[20]. It is analogous with the HRP-catalyzed oxidation of DPD (*N*,*N*-dimethyl-p-phenylenediamine) by H_2O_2, which is a standard method for the photometric determination of H_2O_2[5]. Based on the well-established HRP chemistry[21], the HRP-catalyzed oxidation of ABTS by H_2O_2 can be summarized by the following eqs S8–S11.

$$\text{HRP (Por-Fe}^{\text{III}}\text{)} + H_2O_2 \rightarrow \text{Compound I } (^{\bullet+}\text{Por-Fe}^{\text{IV}}\text{=O}) + H_2O \quad \text{(S8)}$$

$$\text{Compound I } (^{\bullet+}\text{Por-Fe}^{\text{IV}}\text{=O}) + \text{ABTS} \rightarrow \text{ Compound II (Por-Fe}^{\text{IV}}\text{=O)} + \text{ABTS}^{\bullet+} \quad \text{(S9)}$$

$$\text{Compound II (Por-Fe}^{\text{IV}}\text{=O)} + \text{ABTS} \rightarrow \text{HRP (Por-Fe}^{\text{III}}\text{)} + \text{ABTS}^{\bullet+} \quad \text{(S10)}$$

$$\text{Net reaction: } H_2O_2 + 2\text{ABTS} \rightarrow 2\text{ABTS}^{\bullet+} \quad \text{(S11)}$$

In the first step, H_2O_2 converts the ferric heme peroxidase (Por-Fe^{III}) into Compound I ($^{\bullet+}$Por-Fe^{IV}=O), which is a porphyrin π-cation radical with an iron(IV) species (eq S8). Compound I is usually reduced by two consecutive one-electron steps to the native ferric enzyme via the intermediate complex Compound II (Por-Fe^{IV}=O). The one-electron oxidation of ABTS by Compound I and Compound II to $ABTS^{\bullet+}$ is shown in eqs S9 and S10, respectively. Overall, one mole of H_2O_2 produces 2 moles of $ABTS^{\bullet+}$.

To confirm the validity of this method, standard curves for H_2O_2 vs. $ABTS^{\bullet+}$ were generated at various pHs (2.9 – 8.8). To 25 mL of buffered solutions containing H_2O_2 (0 – 24 μM) and ABTS (80 μM), 50 μL of HRP stock solution (1 mg mL^{-1}) was added. Increase of the absorbance at 415 nm (ΔA_{415}) was measured 5 min after the addition of HRP and the formation of $ABTS^{\bullet+}$ was calculated by eq S6. The $ABTS^{\bullet+}$ formation was typically completed within 3 min after the

addition of HRP and the formed $ABTS^{\bullet+}$ was stable for > 30 min (absorbance changes at 415 nm were less than 5 %). Figure SI-11 clearly shows that at the tested pHs of 4.2, 7.0, and 8.8, one mole of H_2O_2 produces 2 moles of $ABTS^{\bullet+}$, which is consistent with the above proposed reaction mechanism (eqs S8 – S11). In addition, standard curves were generated in presence of 20 μM of Fe(III), 10 μM of $ABTS^{\bullet+}$, or a sample after reaction of 20 μM of Fe(VI) with 80 μM of ABTS at pH 7. The results confirm that these matrix components (e.g., Fe(III) and $ABTS^{\bullet+}$) do not interfere with the reaction stoichiometry.

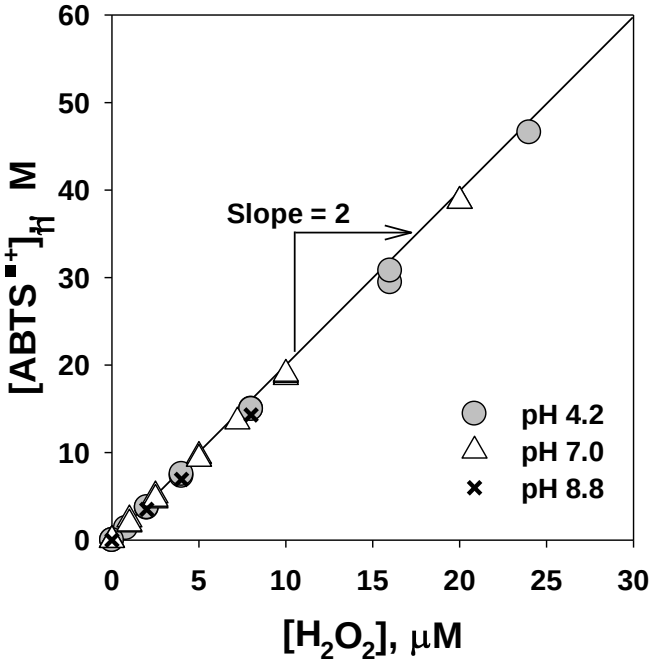

Figure SI-11. Formation of $ABTS^{\bullet+}$ by a HRP-catalyzed oxidation of ABTS by H_2O_2 at pHs of 4.2, 7.0, and 8.8. Experimental conditions: $[H_2O_2]_0$ = 0 – 24 μM, $[ABTS]_0$ = 80 μM, $[HRP]_0$ = 2 mg L^{-1} at pH 4.2 (10 mM phosphate/10 mM acetate), 7.0 (10 mM phosphate), and 8.8 (10 mM phosphate/10 mM borate).

Use of the HRP/ABTS method to determine H_2O_2 formation from the ferrate(VI)-ABTS reaction is advantageous because the system already contains residual ABTS after the completion of the ferrate(VI)-ABTS reaction. Accordingly, 50 μL of the HRP stock solution (1 mg mL^{-1}) was added into 25 mL of a solution where the ferrate(VI)-ABTS reaction was completed. The increase of the absorbance at 415 nm (ΔA_{415}) was measured 5 min after the addition of HRP and the formation of H_2O_2 was calculated by eq S12.

$$\Delta[H_2O_2]_{produced} = \frac{1}{2}\frac{\Delta A_{415}}{\varepsilon_{ABTS\bullet+,415}\,\ell} \quad \text{(S12)}$$

3) Final iron oxidation state. To confirm the final oxidation state of iron (Fe(III) vs. Fe(II)), 0.5 mL of a bipyridine (BPY) stock solution (5 mM) was added to the reaction solution (25 mL) after completion of the ferrate(VI)-ABTS reaction at pH 4.2 and 7.0. BPY forms a complex with Fe(II) that has a maximum absorption at 552 nm (ε = 8650 M^{-1} cm^{-1})[4]. The absorbance change at 552 nm after addition of BPY was negligible, indicating that Fe(III) not Fe(II) is the final product from the ferrate(VI)-ABTS reaction.

SI-Text-3.2. Self-decomposition of ferrate(VI)

1) Formation of H_2O_2 and O_2. 100 mL solutions were prepared at pH 7 using 10 mM (for $[Fe(VI)]_0$ < 300 μM) or 50 mM phosphate buffer (for $[Fe(VI)]_0$ > 300 μM). These solutions were purged by a N_2 stream for > 30 min to remove aqueous O_2 ($[O_2]_0$ < 10 μM) and then transferred to a 110 mL flask with a stopper. The reaction was initiated by adding a known amount of $K_2Fe^{VI}O_4$ powder to the buffered, O_2-free solutions under vigorous stirring. The applied initial ferrate(VI) concentrations were 40 – 810 μM. To minimize O_2 introduction, the flask was always closed by a stopper except for the moment of ferrate(VI) addition. In addition, the stirring was stopped immediately after complete mixing of the added ferrate(VI). Blank tests showed that increases of the O_2 concentration were less than 5 μM after 1 hr. After near-completion of the reaction, the reaction solutions were analyzed for O_2, H_2O_2 and residual ferrate(VI) concentrations. The reaction time was given to allow more than a 95% decrease of the initial ferrate(VI) concentration, spaning from 5 to 120 min depending on the initial ferrate(VI) concentration. The reaction time was pre-calculated based on the ferrate(VI) self-decomposition rate constant at pH 7 ($k_{app\text{-}self}$ = 54 M^{-1} s^{-1}) and the applied initial ferrate(VI) concentration. Aqeuous O_2 concentrations were determined by an O_2 meter (CellOx 325 electrode, Oxi 340, WTW, Weilheim, Germany) immediately after completion of the reaction. Residual ferrate(VI) concentrations were determined by the ABTS method[3], confirming that ferrate(VI) had decreased >95% of its initial concentration. H_2O_2 concentrations were determined by the HRP-ABTS method. Since the reaction of ferrate(VI) with ABTS produces H_2O_2 (i.e., 0.93 moles of H_2O_2 per mole of ferrate(VI) at pH 4.2 where the ABTS method is performed), the H_2O_2 produced from the ferrate(VI)-ABTS reaction was subtracted from the determined overall H_2O_2 concentration by

the HRP-ABTS method. In all cases, the fraction of H_2O_2 produced from the ferrate(VI)-ABTS reaction was less than 5 % of the H_2O_2 formation from the ferrate(VI) self-decomposition.

2) Quantification of superoxide radical ($O_2^{\bullet-}$) formation-the TNM assay. The formation of $O_2^{\bullet-}$ has been checked and quantified by its fast reaction with tetranitromethane (TNM = $C(NO_2)_4$, eq S16) by measuring the formation of the nitroform anion, $C(NO_2)_3^-$ (NF^-, ε = 15,000 M^{-1} cm^{-1} at 350 nm)[22]. This is a common technique in peroxyl radical chemistry[23] but has also been applied to ozone chemistry[22,24] to determine the formation of $O_2^{\bullet-}$.

$$O_2^{\bullet-} + C(NO_2)_4 \rightarrow O_2 + C(NO_2)_3^- + NO_2^{\bullet} \qquad k_{S13} = 2\times10^9 \ M^{-1}\ s^{-1} \qquad (S13)$$

To quantifiy the $O_2^{\bullet-}$ formation from the self-decomposition of ferrate(VI), UV-Vis absorption spectra of a series of solutions containing Fe(VI) (40 μM), H_2O_2 (40 μM), TNM (400 μM), and combinations thereof were measured at pH 7 (Figure SI-12). These solutions include: a) Fe(VI)/H_2O_2/TNM, b) Fe(VI)/TNM, c) Fe(VI)/H_2O_2, d) Fe(VI), e) H_2O_2/TNM, and f) TNM. The prepared solutions were allowed to react for 60 min and the UV-Vis absorption was measured in a 5 cm cell. UV-Vis absorption measurements for those multiple composition solutions were necessary because the final iron product Fe(III) has a strong absorption near 350 nm and interferes with the spectrum of NF^-. Note that 40 μM of Fe(VI) at pH 7 was decomposed > 90 % by its self-decomposition after 60 min, and produces ~12 μM of H_2O_2 (see Figure 6 in the main text). Therefore, the UV-Vis absorption spectra of a solution containing (c) Fe(VI)/H_2O_2 and (d) Fe(VI) are mainly from the Fe(III)-phosphate complex. In addition, the (f) TNM solution shows a weak absorption near 350 nm, therefore this background spectrum should be considered when estimating $O_2^{\bullet-}$ formation. The spectrum of a solution containing (e) H_2O_2/TNM shows that H_2O_2 reacts slowly with TNM, producing 0.4 μM of NF^- in 60 min. Based on this, the second-order rate constant (k) for the reaction of H_2O_2 and TNM at pH 7 is estimated to be ~0.7×10^{-2} M^{-1} s^{-1}. Sager and Hoffsommer[25] investigated the kinetics and mechanism of this reaction and reported the k = 1.1×10^3 M^{-1} s^{-1} for eq S14. This corresponds to an apparent k of 2.8×10^{-2} M^{-1} s^{-1} at pH 7 (pK_a of H_2O_2 is 11.6), which is similar to the rate constant measured in this study (a factor of 2.5 difference).

$$HO_2^- + C(NO_2)_4 \rightarrow O_2 + C(NO_2)_3^- + NO_2^{\bullet} + H^+ \qquad k_{S17} = 1.1\times10^3 \ M^{-1}\ s^{-1} \qquad (S14)$$

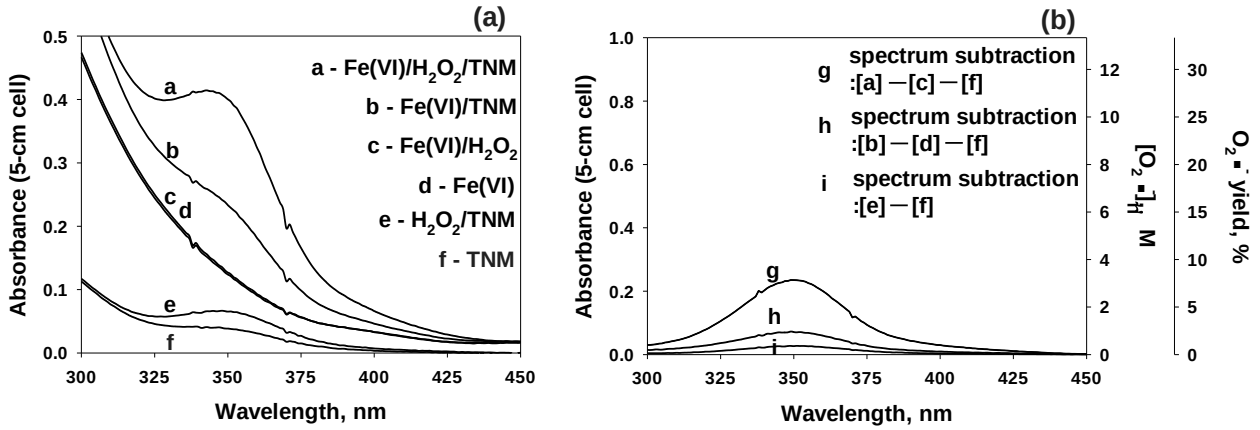

Figure SI-12. UV-Vis absorption spectra of solutions containing Fe(VI) (40 μM), H_2O_2 (40 μM), TNM (400 μM), and combinations thereof after 60 min reaction time in buffered solutions at pH 7 (25 mM phosphate buffer). Note that the self-decomposition of 40 μM ferrate(VI) at pH 7 is > 90 % after 60 min, leaving ~12 μM of H_2O_2 (see Figure 6 in the main text). (a) UV absorption spectra of each combination set, and (b) UV absorption spectra obtained by subtracting spectra from each combination set to show the magnitude of $C(NO_2)_3^-$ formation (NF^-, ε = 15,000 M^{-1} cm^{-1} at 350 nm)[22].

The formation of $O_2^{\bullet-}$ during the self-decomposition of 40 μM ferrate(VI) at pH 7 could be estimated from the UV absorption spectra of 'b', 'd', and 'f'. Since (d) Fe(VI) and (f) TNM solutions are contributing to the UV absorption at 350 nm, the spectra of (d) Fe(VI) and (f) TNM were substracted from (b) Fe(VI)/TNM. The resulting spectrum (curve h = b – d – f) is shown in Figure SI-12b and consistent with the known spectrum of NF^-. From the UV absorption increase at 350 nm, the $O_2^{\bullet-}$ formation was determined to be 0.9 μM, which corresponds to a 2.4 % yield based on the initial Fe(VI) concentration (40 μM). If we consider the contribution of H_2O_2 (~12 μM from ferrate(VI) self-decomposition, see Figure 6 in the main text) to the NF^- formation, the actual yield of $O_2^{\bullet-}$ is expected to be lower than 2.4 %. The formation of $O_2^{\bullet-}$ during the reaction of ferrate(VI) with H_2O_2 (40 μM each) at pH 7 could also be estimated from the UV absorption spectra of 'a', 'c', and 'f' (curve g = a – c – f). In presence of H_2O_2, the yield of $O_2^{\bullet-}$ was estimated to be < 8% of the initial ferrate(VI) concentration. Overall, the $O_2^{\bullet-}$ formation during the ferrate(VI) self-decomposition was found to be insignificant (below 2% yield).

3) Quantification of hydroxyl radical ($^{\bullet}$OH) formation-the pCBA and tert-BuOH assay. To check whether $^{\bullet}$OH is produced during the self-decomposition of ferrate(VI), a probe compound

for $^{\bullet}$OH was used. *Para*-chloro benzoic acid (*p*CBA) has been widely used as a probe compound for $^{\bullet}$OH in ozone- or UV-based advanced oxidation processes[26]. *p*CBA is resistent to oxidation by ferrate or other oxidants such as ozone but reactive to $^{\bullet}$OH with a second-order rate constant of 5×10^{9} M^{-1} s^{-1} [26]. Transformation of *p*CBA (initial concentration 1 μM) was tested in pure solution at pH 7 (5 mM phosphate buffer solution) after treatment with ferrate(VI) at initial concentrations of 25, 50, and 100 μM. The *p*CBA transformation was less than 3 %, indicating that the $^{\bullet}$OH formation during ferrate(VI) self-decay is low.

$^{\bullet}$OH formation was also determined by measuring formaldehyde formation in presence of an excess of *tert*-butanol[22]. In an excess of *tert*-butanol (1 mM in this study), most $^{\bullet}$OH, if produced, react with *tert*-butanol (k = 6×10^{8} M^{-1} s^{-1})[22] that produces several products including formaldehyde. Therefore, by measuring the formaldehyde, the $^{\bullet}$OH formation can be estimated. Figure SI-13 shows the formation of formaldehyde as a function of time (4, 24, and 72 hr) during ferrate(VI) self-decomposition with initial ferrate(VI) concentrations of 25, 50 and 100 μM in phosphate buffered solution at pH 7 in presence of 1 mM of *tert*-butanol. Formaldehyde formation increased with the initial ferrate(VI) concentration and was 0.4–0.7 μM, 0.8–1.0 μM, and 1.9–2.5 μM for initial ferrate(VI) concentrations of 25, 50, and 100 μM, respectively. With an assumption that the formaldehyde yield from the reaction of $^{\bullet}$OH with *tert*-butanol is 0.5 (this is determined in a system using ozone as $^{\bullet}$OH source[22]), the $^{\bullet}$OH formation and yields were also calculated. In all tested conditions, the % $^{\bullet}$OH yields ($[^{\bullet}OH]/[Fe(VI)]_0\times100$) were less than 5.3%. Overall, from the *p*CBA and *tert*-butanol assays, the $^{\bullet}$OH formation from the self-decomposition of ferrate(VI) is concluded to be insignificant (less than 5% yield).

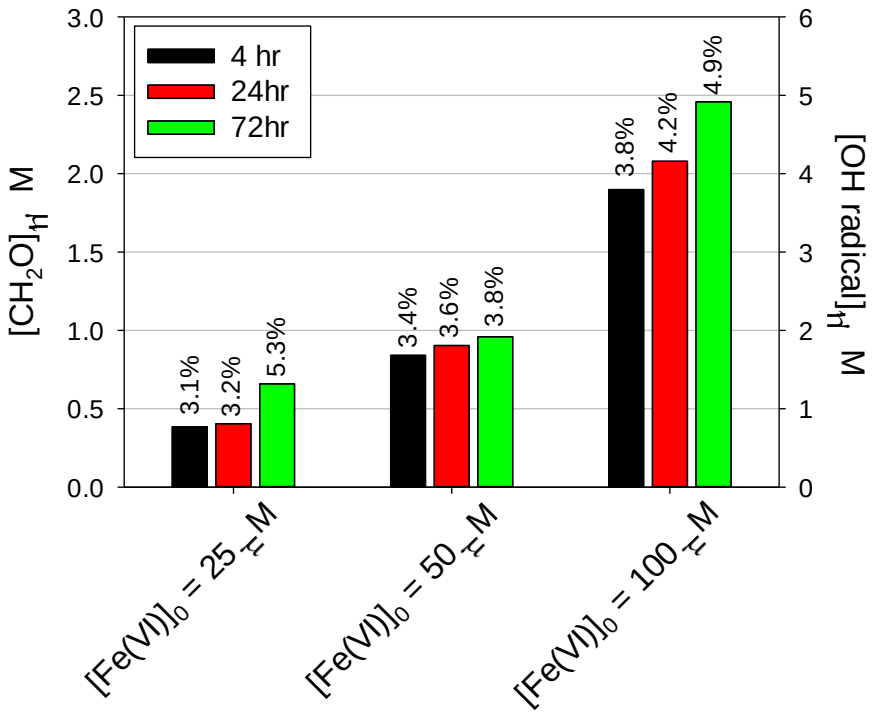

Figure SI-13. Formation of formaldehyde during ferrate(VI) self-decomposition in phosphate buffer solution at pH 7 in presence of 1 mM *tert*-butanol. $^{\bullet}$OH formation is assumed to be twice the formaldehyde formation. The numbers above the bars represent % yield of $^{\bullet}$OH based on the initial ferrate(VI) concentration.

4) Final iron oxidation state. To confirm the final oxidation state of iron (Fe(III) vs. Fe(II)), 0.5 mL of a bipyridine (BPY) stock solution (5 mM) was added to the reaction solution (25 mL) during the self-decay of 100 μM ferrate(VI) at pH 7 (t = 1, 5, 10 and 30 min). The absorbance change at 522 nm responsible for the Fe(II)-BPY complex (ε = 8650 M^{-1} cm^{-1})[4] after addition of BPY was negligible, indicating that Fe(III) not Fe(II) is the final product from the ferrate(VI) self-decay. Carr et al[27] observed a Fe(II)-phenanthroline complex formation upon addition of phenanthroline to a ferrate(VI) self-decayed solution and proposed Fe(II) as major product. In contrast, Rush et al[14] did not observe a Fe(II) formation in a similar experiment. Instead, they found Fe(II) formation upon addition of phenanthroline to a solution containing Fe(III) and H_2O_2, indicating that Fe(II) could have been indirectly produced by reactions of H_2O_2 (from the ferrate(VI) self-decay) with the Fe(III)-phenanthroline complex.

SI-Text-3.3. Stochiometry of the oxidation of Fe(II) by ferrate(VI)

A N_2-purged solution containing 56 μM of Fe(II) was prepared and buffered at pH 6.8 (5 mM carbonate). Auto-oxidation of Fe(II) by O_2 was found to be minimal within 20 min in this N_2-purged solution. Oxidation of Fe(II) by ferrate(VI) was performed in a batch reactor (25 mL) by adding a ferrate(VI) stock solution (~500 μM, pH 9.2 without any buffers) to the solutions containing Fe(II) to achieve initial ferrate(VI) concentrations of 0 – 40 μM. After the addition of ferrate(VI) with mixing, the reaction solution was immidiately analyzed for the remaining Fe(II) (within 1min) by the ferrozine method[4]. Figure SI-14 shows the remaining Fe(II) concentration after oxidation of Fe(II) by varying initial concentration of ferrate(VI). 3 moles of Fe(II) were consumed by each mole of ferrate(VI) (i.e., 1:3 stoichiometry for ferrate(VI):Fe(II)).

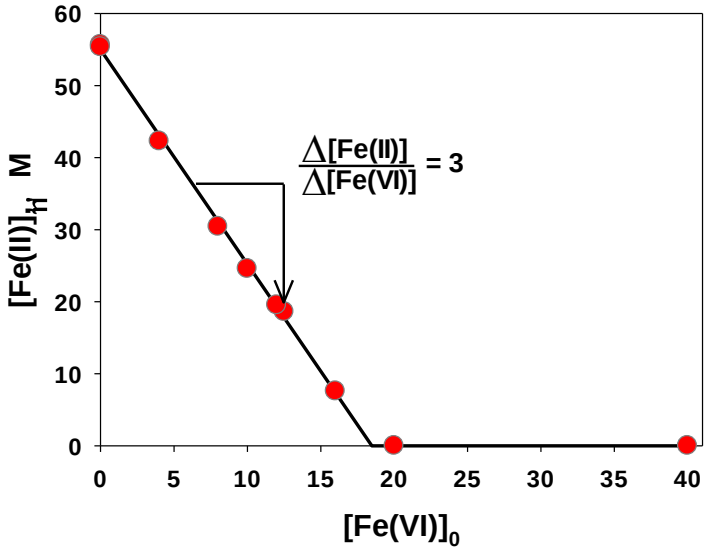

Figure SI-14. Decrease of Fe(II) as a function of the Fe(VI) dose after oxidation of Fe(II) by ferrate(VI) in a N_2-purged aqueous solution buffered at pH 6.8 (5 mM carbonate). Symbols represent the measured data and the line represents the theoretical 1:3 stoichiometric relationship for ferrate(VI):Fe(II).

SI-Text-4. Kinetic simulation

Kintecus[28], a chemical kinetic simulator, was used to simulate the reaction of Fe(VI) with ABTS and the ferrate(VI) self-decay.

SI-Text-4.1. Reaction of ferrate(VI) with ABTS

Four reactions (eqs 9 – 12 in the main text, Table 1) are proposed for the ferrate(VI)-ABTS system.

$$HFe^{VI}O_4^- + ABTS + H^+ \rightarrow H_2Fe^{V}O_4^- + ABTS^{\bullet+} \qquad k_9 \qquad (9)$$

$$H_2Fe^{V}O_4^- + H_2O + H^+ \rightarrow Fe^{III}(OH)_3(aq) + H_2O_2 \qquad k_{10} \qquad (10)$$

$$2H_2Fe^{V}O_4^- + 2H_2O + 2H^+ \rightarrow 2Fe^{III}(OH)_3(aq) + 2H_2O_2 \qquad k_{11} \qquad (11)$$

$$H_2Fe^{V}O_4^- + H_2O_2 + H^+ \rightarrow Fe^{III}(OH)_3(aq) + O_2 + H_2O \qquad k_{12} \qquad (12)$$

The second-order rate constants, k_9, for the reaction of ferrate(VI) with ABTS have been determined in this study in the pH range of 1.5 – 10 (see Figure 1 in the main text or Figure SI-15). Reactions 10 and 11 represent the decay of perferryl(V). The kinetics of the reactions were investigated previously by pulse-radiolysis[10,11]. According to these studies, perferryl(V) decays by first-order or second-order kinetics with respect to perferryl(V) depending on pH and perferryl(V) concentration. At acidic pH and low perferryl(V) concentration (e.g. pH < 7 and [Fe(V)] < 1 μM), perferryl(V) decays mainly by first-order kinetics, but the mode of decay changes to second-order kinetics at basic pH and high perferryl(V) concentrations (e.g. pH > 9 and [Fe(V)] > 1 μM). Perferryl(V) has been proposed to undergo the following acid-base reactions (eqs S15 – S17) in aqueous solution.

$$H_3Fe^{V}O_4 \rightleftharpoons H_2Fe^{V}O_4^- + H^+ \qquad pK_{S15} = \sim 6.0^{11} \qquad (S15)$$

$$H_2Fe^{V}O_4^- \rightleftharpoons HFe^{V}O_4^{2-} + H^+ \qquad pK_{S16} = 7.2^{11} \qquad (S16)$$

$$HFe^{V}O_4^{2-} \rightleftharpoons Fe^{V}O_4^{3-} + H^+ \qquad pK_{S17} = 10.1^{11} \qquad (S17)$$

The first-order decay of perferryl(V) is described by the following species-specific reactions[11]:

$$H_3Fe^{V}O_4\ (T_d) + H_2O \rightleftharpoons Fe^{V}(OH)_5(H_2O)\ (O_h) \qquad K_{S18}\ (=k_{S18f}/\ k_{S18b}) \qquad (S18f, S18b)$$

$$Fe^{V}(OH)_5(H_2O)\ (O_h) + H^+ \rightleftharpoons Fe^{V}(OH)_4(H_2O)_2^+ \qquad K_{S19}\ (=k_{S19f}/\ k_{S19b}) \qquad (S19f, S19b)$$

$$Fe^{V}(OH)_4(H_2O)_2^+ \rightarrow Fe^{III}(OH)_3(aq) + H_2O_2 + H_2O + H^+ \qquad k_{S20} \qquad (S20)$$

$$H_2Fe^{V}O_4^- + 2H_2O \rightarrow Fe^{III}(OH)_3(aq) + H_2O_2 + OH^- \qquad k_{S21} \qquad (S21)$$

$$HFe^{V}O_4^{2-} + 3H_2O \rightarrow Fe^{III}(OH)_3(aq) + H_2O_2 + 2OH^- \qquad k_{S22} \qquad (S22)$$

Reactions S18 – S20 are proposed to explain the strong pH-dependent increase of the first order decay rate of Fe(V) by a factor of 10^3 with a decrease of pH from 6.5 to 5[11]. It was hypothesized that the $H_3Fe^{V}O_4$ species with a tetrahedral (T_d) coordination sphere can be converted rapidly into $Fe^{V}(OH)_5(H_2O)$ (O_h) species with an expanded octahedral (O_h) coordination sphere (eq S18). The $Fe^{V}(OH)_5(H_2O)(O_h)$ species undergoes protonation (eq S19) prior to its decomposition to ferric

ion and H_2O_2 (eq S20). Reactions S21 and S22 represent the first order decay of $H_2Fe^{V}O_4^{-}$ and $HFe^{V}O_4^{2-}$ species to ferric ion and H_2O_2, respectively. By assuming a rapid equilibrium between the tetrahedral forms of Fe(V) species (eqs S15 – S17) and by applying the steady-state approximation to the octahedral species (eqs S18 and S19), the overall first-order decay kinetics of Fe(V) can be expressed as eqs S23 and S24.

$$-\mathrm{d[Fe(V)]/dt} = k_{10}[\mathrm{Fe(V)}] \qquad \text{(S23)}$$

$$k_{10} = (A[H^+]^2\alpha\{H_3Fe^{V}O_4\})/(B + C[H^+] + D[H^+]^2) + k_{S21}\alpha\{H_2Fe^{V}O_4^{-}\} + k_{S22}\alpha\{HFe^{V}O_4^{2-}\} \qquad \text{(S24)}$$

where $\alpha\{H_3Fe^{V}O_4\}$, $\alpha\{H_2Fe^{V}O_4^{-}\}$, and $\alpha\{HFe^{V}O_4^{2-}\}$ represent the fraction of $H_3Fe^{V}O_4$, $H_2Fe^{V}O_4^{-}$, and $HFe^{V}O_4^{2-}$ species, respectively, which are calculated from the equilibria, eqs S15 – S17, and the parameters, A– D which are obtained from the steady-state treatment, where $A = k_{S18f}\,k_{S19f}\,k_{S20}$, $B = k_{S18b}\,k_{S19b}$, $C = k_{S19f}\,k_{S19b} + k_{S18b}\,k_{S20}$, and $D = k_{S19f}\,k_{S20}$. Based on the fitting of experimental data with the model (i.e., eq S24), the obtained values were: $A = 7.0\times10^{20}$ M^{-2} s^{-3}, $B = = 3.8\times10^{4}$ s^{-2}, $C = 1.8\times10^{9}$ M^{-1} s^{-2}, $D = 1.0\times10^{6}$ M^{-2} s^{-2}, $k_{S26} = 150$ s^{-1}, and $k_{S27} = 5$ s^{-1} (further details can be found in the original reference). Figure SI-15 shows the calculated first-order decay of Fe(V) (k_{10}) as a function of pH.

The second-order decay of perferryl(V) (reaction 11) is described by the following species-specific reactions (eqs S25 – S28) and the overall second-order decay kinetics of perferryl(V) can be expressed as eqs S29 and S30[10].

$$H_2Fe^{V}O_4^{-} + H_2Fe^{V}O_4^{-} + 7H_2O \rightarrow 2Fe^{III}(OH)_3(aq) + 2H_2O_2 + 2OH^- \qquad k_{S25} \qquad \text{(S25)}$$

$$H_2Fe^{V}O_4^{-} + HFe^{V}O_4^{2-} + 8H_2O \rightarrow 2Fe^{III}(OH)_3(aq) + 2H_2O_2 + 3OH^- \qquad k_{S26} \qquad \text{(S26)}$$

$$HFe^{V}O_4^{2-} + HFe^{V}O_4^{2-} + 9H_2O \rightarrow 2Fe^{III}(OH)_3(aq) + 2H_2O_2 + 4OH^- \qquad k_{S27} \qquad \text{(S27)}$$

$$HFe^{V}O_4^{2-} + Fe^{V}O_4^{3-} + 10H_2O \rightarrow 2Fe^{III}(OH)_3(aq) + 2H_2O_2 + 5OH^- \qquad k_{S28} \qquad \text{(S28)}$$

$$-\mathrm{d[Fe(V)]/dt} = 2k_{11}[\mathrm{Fe(V)}] \qquad \text{(S29)}$$

$$k_{11} = k_{S28}\alpha\{H_2Fe^{V}O_4^{-}\}^2 + k_{S29}\alpha\{H_2Fe^{V}O_4^{-}\}\alpha\{HFe^{V}O_4^{2-}\} + k_{S30}\alpha\{HFe^{V}O_4^{2-}\}^2 + k_{S31}\alpha\{HFe^{V}O_4^{2-}\}\alpha\{Fe^{V}O_4^{3-}\} \qquad \text{(S30)}$$

Based on the fitting of experimental data with the model (i.e., eq S30), the obtained values were: $k_{S25} = 9\times10^{7}$ M^{-1} s^{-1}, $k_{S26} = 3\times10^{7}$ M^{-1} s^{-1}, $k_{S27} = 1.5\times10^{7}$ M^{-1} s^{-1}, and $k_{S28} = 1\times10^{7}$ M^{-1} s^{-1} [10]. Figure SI-15 also shows the calculated pH-dependent seconder-order decay of perferryl(V) (k_{11}).

The second-order rate constants for the reaction of perferryl(V) with H_2O_2 (reaction 12) were also determined by Bielski and co-workers using pulse-radiolysis[14]. The acid-base equilibrium of

H_2O_2 (eq S3) and the species-specific reactions can describe the overall reaction between perferryl(V) and H_2O_2 species (eqs S31 – S34).

$$H_2Fe^{V}O_4^{-} + H_2O_2 \rightarrow Fe^{III}(OH)_3(aq) + O_2 + OH^{-} \qquad k_{S31} \qquad (S31)$$

$$HFe^{V}O_4^{2-} + H_2O_2 + H_2O \rightarrow Fe^{III}(OH)_3(aq) + O_2 + 2OH^{-} \qquad k_{S32} \qquad (S32)$$

$$HFe^{V}O_4^{2-} + HO_2^{-} + 2H_2O \rightarrow Fe^{III}(OH)_3(aq) + O_2 + 3OH^{-} \qquad k_{S33} \qquad (S33)$$

$$Fe^{V}O_4^{3-} + HO_2^{-} + 3H_2O \rightarrow Fe^{III}(OH)_3(aq) + O_2 + 4OH^{-} \qquad k_{S34} \qquad (S34)$$

The pH-dependent second-order rate constant, k_{12}, is expressed by eq S35 and its calculated values as a function of pH are shown in Figure SI-15.

$$k_{12} = k_{S31}\alpha\{H_2Fe^{V}O_4^{-}\}\beta\{H_2O_2\} + k_{S32}\alpha\{HFe^{V}O_4^{2-}\}\beta\{H_2O_2\} + k_{S33}\alpha\{HFe^{V}O_4^{2-}\}\beta\{HO_2^{-}\} + k_{S34}\alpha\{Fe^{V}O_4^{3-}\}\beta\{HO_2^{-}\} \qquad (S35)$$

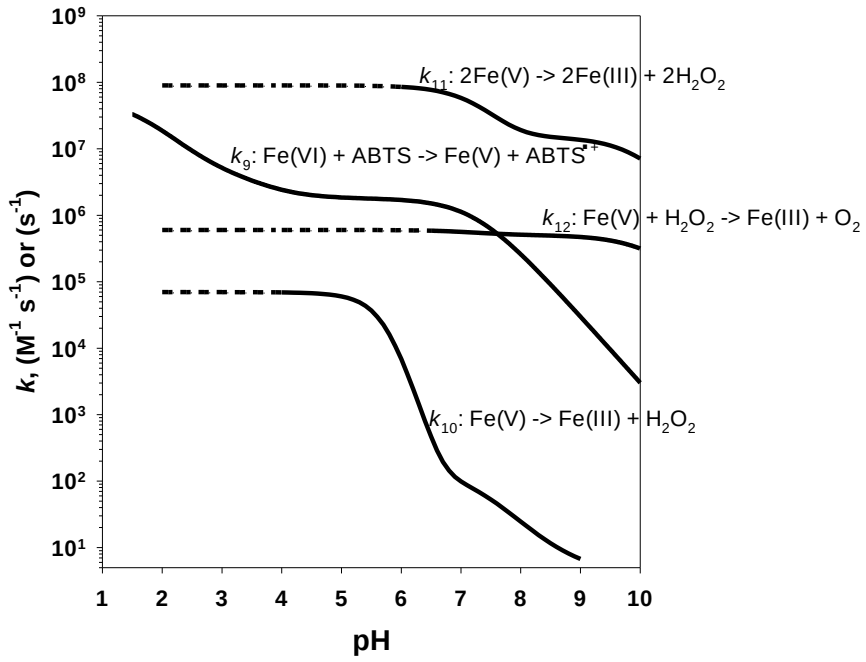

Figure SI-15. Summary of the rate constants for the reactions in the ferrate(VI)-ABTS system. The second-order rate constants, k_9 (Fe(VI) + ABTS $\rightarrow$ Fe(V) + $ABTS^{\bullet+}$) were determined in the present study. The first-order rate constants, k_{10} (Fe(V) $\rightarrow$ Fe(III) + H_2O_2) and the second-order rate constants, k_{11} (2Fe(V) $\rightarrow$ 2Fe(III) + $2H_2O_2$) and k_{12} (Fe(V) + H_2O_2 $\rightarrow$ Fe(III) + O_2) were determined previously[10,11,14] and reproduced here based on the corresponding species-specific rate constants. The continuous-lines represent *k*-values that are experimentally measured and the dashed lines represent *k*-values that are extrapolated based on the corresponding kinetic models.

Based on reactions 9 – 12 and the corresponding reaction rate information (Figure SI-15), a kinetic model was constructed and simulated by using the Kintecus program[28]. H_2O_2 formation was simulated for the reaction of 0 – 25 μM of Fe(VI) with 80 μM of ABTS in the pH range 2 – 10. Figure SI-16 shows the selected data by comparing the measured and predicted H_2O_2 formation from the reaction of Fe(VI) with ABTS as a function of the initial Fe(VI) concentration. The kinetic model could reproduce the key feature of the reaction of Fe(VI) with ABTS, that is, the decreasing H_2O_2 yield with increasing pH. However, the kinetic model over-predicted the H_2O_2 formation at any given pH. In addition, at pH > 9 the predicted H_2O_2 formation deviated from the linear increase for increasing initial ferrate(VI) concentrations.

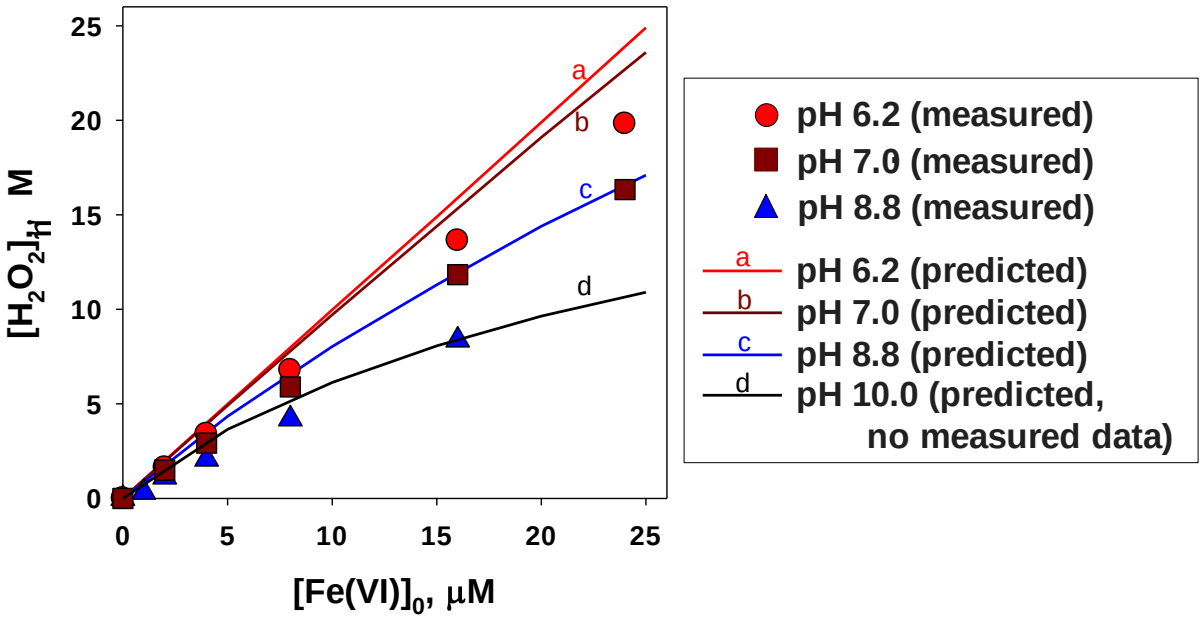

Figure SI-16. Measured (symbols) and predicted (lines) H_2O_2 formation from the reaction of ferrate(VI) with ABTS (initial 80 μM) as a function of the initial ferrate(VI) concentration (0 – 25 μM) and pH (6.2, 7.0, 8.8 and 10.0).

From the slope of the linear regressions for the H_2O_2 formation versus the initial ferrate(VI) concentration, the H_2O_2 yields were obtained at different pHs and compared with the experimental values. Figure 3 in the main text shows that the developed kinetic model can represent reasonably the pH-dependence of the H_2O_2 yield even though the predicted H_2O_2 yields are up to 26% higher than the measured values. Considering that each of the rate constants, k_9, k_{10},

k_{11}, and k_{12} were determined separately in different experimental conditions, the agreement between the simulated and measured values shown in Figure 3 is reasonable.

Because perferryl(V) has a higher reactivity than ferrate(VI), one would expect a reaction of perferryl(V) with ABTS in the ferrate(VI)-ABTS system. However, the reaction of perferryl(V) with ABTS is not consistent with the observed 1:1 stoichiometry for the ferrate(VI) consumption and $ABTS^{\bullet+}$ formation (Figure 2 in the main text). This 1:1 stoichiometry was observed when the initial ABTS concentration increased from 80 μM up to 400 μM at pH 4.2 (data not shown). The upper limit for the second-order rate constant for the reaction of perferryl(V) with ABTS ($k_{Fe(V)\text{-}ABTS}$) could be estimated to be ~3×10^9 M^{-1} s^{-1} at pH 4.2. This is based on the assumption that the initial consumption rate of perferryl(V) by ABTS is at least five-fold lower than the self-decay rate of perferryl(V), i.e., $5\times k_{Fe(V)\text{-}ABTS}[ABTS]_0 < k_{10}$ with $[ABTS]_0$ = 400 μM and $k_{10} = 7\times10^4$ s^{-1}.

SI-Text-4.2. Ferrate(VI) self-decay and the reaction of ferrate(VI) with H_2O_2

The kinetic model for the ferrate(VI) self-decay is comprised of reactions 10 and 12–16 in Table 1 (main text). Kinetic simulations were performed mainly at pH 7 and compared with experimental data. The kinetic aspects of each reaction in Table 1 are discussed in the main text. In the kinetic model, the oxidation of Fe(II) by perferryl(V) or ferryl(IV) is not considered as these reactions are not important during ferrate(VI) self-decay due to the rapid oxidation of Fe(II) by ferrate(VI) ($k_{15} = 10^7$ M^{-1} s^{-1}, Table 1). Kinetic modeling trials showed that the reaction of ferrate(VI) with Fe(II) outcompetes the reaction of perferryl(V) with Fe(II) even when k_{15} is 10^{10} M^{-1} s^{-1}. This is because the perferryl(V) concentration is quite low ([Fe(V)]/[Fe(VI)] = ~5×10^{-5}) due to its rapid self-decay (k_{10} = 100 s^{-1}, Table 1). Regarding ferryl(IV), its concentration is determined by the reaction of ferryl(IV) with H_2O_2 ($k_{14} = 10^4$ M^{-1} s^{-1}, Table 1). From the kinetic model, [Fe(IV)]/[Fe(VI)] is estimated to be ~0.02. Accordingly, the reaction of ferrate(VI) with Fe(II) can still outcompete the reaction of ferryl(IV) with Fe(II) as long as k_{14} is lower than 10^8 M^{-1} s^{-1}. The k_{14} value for the reaction of ferryl(IV) with Fe(II) at pH 7 is currently unknown. At pH 10, k_{14} was reported to be 1.6×10^6 M^{-1} s^{-1} [29]. At pH 0 – 2, k_{14} was reported to be 1.4×10^5 M^{-1} s^{-1} [13]. Therefore, the k_{14} value for the reaction of ferryl(IV) with Fe(II) at pH 7 is not expected to be larger than 10^8 M^{-1} s^{-1} even considering the pH difference. Sensitivity analysis also showed that the reaction of perferryl(V) or ferryl(IV) with Fe(II) are not important in the ferrate(VI) self-decay model.

The developed kinetic model was used to predict the formation of O_2 and H_2O_2 from the self-decay of ferrate(VI) as a function of the initial ferrate(VI) concentration (Figure 5 in the main text). Figure SI-17 shows the same data in Figure 5 in terms of % formation of O_2 and H_2O_2. Figure SI-17 also shows the % formation of H_2O_2 at pH 3.3 after complete consumptions of ferrate(VI).

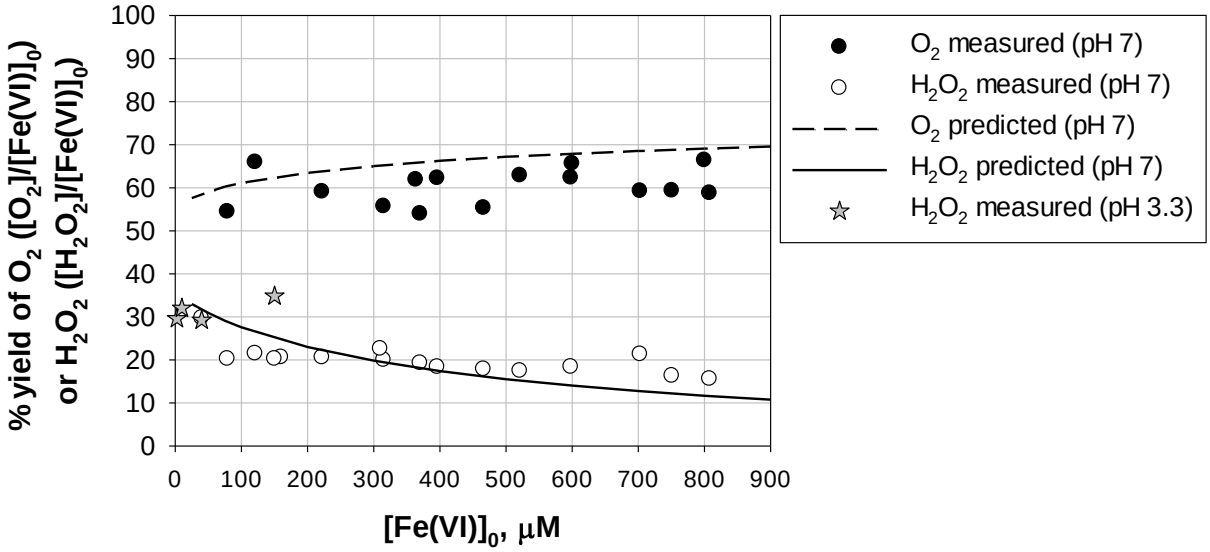

Figure SI-17. % formation yields of O_2 ($\Delta[O_2]/[Fe(VI)]_0\times100$) and H_2O_2 ($\Delta[H_2O_2]/[Fe(VI)]_0\times100$) from the self-decay of ferrate(VI) as a function of the initial ferrate(VI) concentration in a phosphate buffer solution at pH 7 (0.05 – 0.1 M) or pH 3.3 (0.01 M). H_2O_2 and O_2 were determined for >95% ferrate(VI) decomposition. O_2 was not determined in the experiments at pH 3.3. The symbols represent the measured data and the lines the model calculations for pH 7.

To validate the proposed ferrate(VI) self-decomposition model, kinetic experiments for the ferrate(VI) self-decomposition and the ferrate(VI) reaction with H_2O_2 were conducted at pH 7 (5 mM phosphate buffer). For the ferrate(VI) self-decomposition, various initial ferrate(VI) concentrations (10, 40, 160, and 300 μM) were applied to a solution buffered at pH 7. For the reaction of ferrate(VI) with H_2O_2, 40 μM of ferrate(VI) was added to a solution containing 20, 40, and 80 μM of H_2O_2 at pH 7, respectively. For both experiments, the concentration change of ferrate(VI) and H_2O_2 were measured as a function of the reaction time. Ferrate(VI) concentrations were determined by the ABTS method[3]. H_2O_2 concentrations were determined by the HRP-ABTS method (see SI-Text-3.1). Since the reaction of ferrate(VI) with ABTS produces

H_2O_2 (i.e. 0.93 mole of H_2O_2 per mole of ferrate(VI) at pH 4.2 where the ABTS method is performed), the H_2O_2 produced from the ferrate(VI)-ABTS reaction was subtracted from the determined overall H_2O_2 concentration by the HRP-ABTS method. Figure 6 in the main text shows the time-dependent concentration changes of ferrate(VI) and H_2O_2 during the self-decay of ferrate(VI) at pH 7. Figure SI-18 shows the time-dependent concentration changes of ferrate(VI) and H_2O_2 during the reaction of ferrate(VI) and H_2O_2. The results show that the kinetic model successfully predicted the kinetic behavior of ferrate(VI) and H_2O_2.

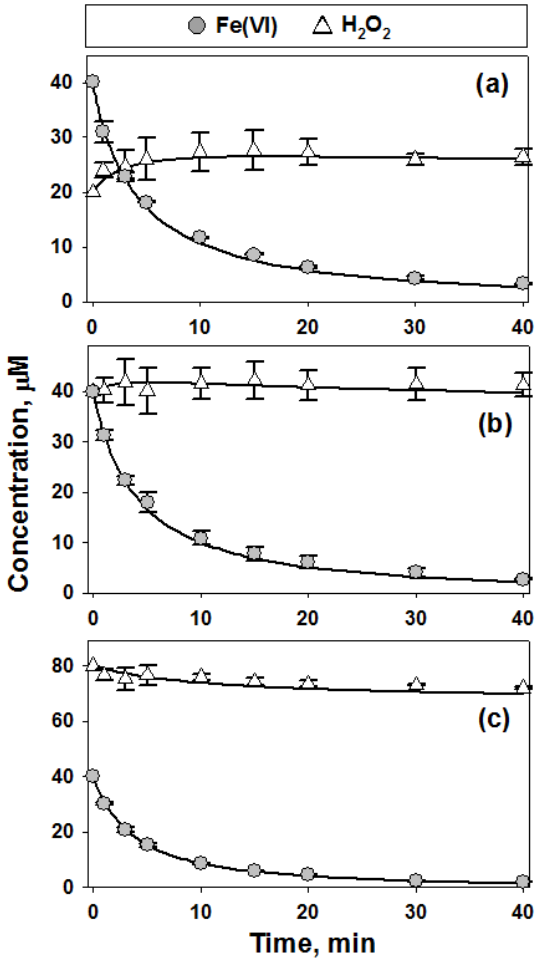

Figure SI-18. Changes of ferrate(VI) and H_2O_2 concentrations during the reaction of 40 μM ferrate(VI) with a) 20 μM, b) 40 μM, and c) 80 μM of H_2O_2 in phosphate buffered solution at pH 7 (5 mM). The symbols represent the measured data and the lines represent model calculations. Error bars represent one standard deviation of data.

References

(1) Thompson, G. W.; Ockerman, G. W.; Schreyer, J. M. *J. Am. Chem. Soc*. **1951**, *73*, 1379–1381.

(2) Bielski, B.H.J.; Thomas, M.J. *J. Am. Chem. Soc*. **1987**, *109*, 7761–7764.

(3) Lee, Y.; Yoon, J.; von Gunten, U. *Wat. Res*. **2005**, *39*, 1946–1953.

(4) Voelker-Bartschat, B. M. *Iron redox cycling in surface waters: effects of humic substances and light.* Ph.D. Thesis; ETH Zürich; Zürich, 1994.

(5) Bader, H.; Sturzenegger, V.; Hoigne, J. *Wat. Res*. **1988**, *22*, 1109–1115.

(6) Lee, Y.; Zimmermann, S. G.; Kieu, A. T.; von Gunten, U. *Environ. Sci. Technol.* **2009,** *43*, 3831–3838.

(7) Buxton, G.V.; Greenstock, C.L.; Helman, W.P.; Ross, W.P. *J. Phys. Chem. Ref. Data* **1988**, *17*, 513–886.

(8) Radiation Chemistry Data Center of the Notre Dame Radiation Laboratroy. Available at http://kinetics.nist.gov/solution/, Universitry of Notre Dame Radiation Laboratory.

(9) Bielski, B.H.J.; Sharma, V.K.; Czapski, G. *Radiat. Phys. Chem.* **1994**, *44*, 479–484.

(10) Rush, J.D.; Bielski, B.H.J. *Inorg. Chem.* **1989**, *28*, 3947–3951.

(11) Rush, J.D.; Bielski, B.H.J. *Inorg. Chem.* **1994,** *33*, 5499–5502.

(12) Jacobsen, F.; Holcman, J.; Sehested, K. *Int. J. Chem. Kinetic.* **1999,** *30*, 215–221.

(13) Logager, T.; Holcman, J.; Sehested, K.; Pedersen, T. *Inorg. Chem.* **1992**, *31*, 3523–3529.

(14) Rush, J. D.; Zhao, Z.; Bielski, B. H. J. *Free Rad. Res.* **1996,** *24*, 187–198.

(15) Sarma, R.; Angeles-Boza, A.M.; Brinkley, D.W.; Roth, J.P. *J. Am. Chem. Soc*. **2012**, *134*, 15371–15386.

(16) Albert, A.; Serjeant, E.P. *The Determination of Ionization Constants: A Laboratory Manual*, 3rd ed.; Chapman & Hall, New York, 1984.

(17) Childs, R. E.; Bardsley, W. G. *Biochemical J*. **1975**, 1*45*, 93–103.

(18) Kadnikova, E.N., Kostic, N.M. *J. Mol. Catal. B: Enzym.* **2002**, *18*, 39–48.

(19) Keesey, J., *Biochemica Information*. 1st Ed.; Boehringer Mannheim Biochemicals; Indianapolis, IN, 1987.

(20) Muller, H. E. *J. Microbiological Methods* **1984**, *2*, 101-102.

(21) Dunford, H. B. *Heme Peroxidases*. John Wiley & Sons: New York, 1999.

(22) Flyunt, R.; Leitzke, A.; Mark, G.; Mvula, E.; Reisz, E.; Schick, R.; von Sonntag, C. *J. Phys. Chem. B* **2003**, *107*, 7242-7253.

(23) von Sonntag, C., Schuchmann, H. -P. *Peroxyl Radicals.* Alfassi, Z. B.; Ed.; Wiley: Chichester: U. K., 1997, pp 173–234.

(24) Sánchez-Polo, M., von Gunten, U., Rivera-Utrilla, J. *Water Res.* **2005**, *39*, 3189-3198.

(25) Sager, W. F., Hoffsommer, J. C. *J. Phys. Chem.* **1969**, *73*, 4155–4162.

(26) Elovitz, M.S.; von Gunten, U. *Ozone Sci. Eng.* **1999**, *21*, 239–260.

(27) Carr, J. D.; Kelter, P. B.; Tabatabai, A.; Splichal, D.; Erickson, J.; McLaughlin, C. W. *Proc. Conf. Water. Chlorin. Chem. Environ. Impact. Health Effects* **1985**, *5*, 1285–1298.

(28) Ianni, J.C. *Kintecus Version 4.55*. www.kintecus.com, 2012.

(29) Melton, J.D.; Bielski, B.H.J. *Radiat. Phys. Chem.* **1990**, *36*, 725–733.